

## Rubidium vapor cell with integrated Bragg reflectors for compact atomic MEMS

Maximillian A. Perez<sup>a,\*</sup>, Uyen Nguyen<sup>b</sup>, Svenja Knappe<sup>c</sup>, Elizabeth A. Donley<sup>c</sup>,  
John Kitching<sup>c</sup>, Andrei M. Shkel<sup>a</sup>

<sup>a</sup> *Microsystems Laboratory, University of California, Irvine, CA, 92697-3975, USA*

<sup>b</sup> *Electrical Engineering and Computer Science, University of California, Berkeley, CA, 94720-1770, USA*

<sup>c</sup> *Time and Frequency Division, National Institute of Standards and Technology, Boulder, CO, 80305-3328, USA*

### ARTICLE INFO

#### Article history:

Received 2 April 2008

Received in revised form 4 February 2009

Accepted 1 June 2009

Available online 9 June 2009

#### PACS:

07.07.Df

33.25.+k

42.79.Fm

42.82.Bq

85.85.+j

#### Keywords:

Atomic MEMS

Optical MEMS

Vapor cells

Bragg reflector

Thin films

PECVD

Magnetometer

Gyroscope

### ABSTRACT

This paper reports on a method for improving the optical efficiency of micromachined reflectors integrated in rubidium vapor cells for application in atomic MEMS sensors. A hybrid bulk micromachining and multilayer PECVD thin film process is used to form the Bragg reflectors on angled sidewalls, which redirect laser light through the vapor cell and back toward the plane of the source with reduced optical power loss. Integrated thin film Bragg reflectors are shown to improve the reflectance of the micromachined surface by almost three times, resulting in an optical return efficiency of two paired dielectric reflectors that is as much as eight times higher than uncoated silicon reflectors. Absorption of the  $^{87}\text{Rb } D_1$  absorption line at a wavelength of 795 nm in a 1 mm<sup>3</sup> vapor cell is demonstrated experimentally by use of two integrated thin film reflectors with a total optical return efficiency approaching 40%.

© 2009 Elsevier B.V. All rights reserved.

### 1. Introduction

The engineering of miniature vapor cells for the encapsulation of gases is of widening interest [1]. Such cells form the central elements in emerging microelectromechanical system (MEMS) technologies based on the atomic transitions of alkali gases, such as miniaturized atomic clocks, magnetometers and potentially gyroscopes [2,3]. Micromachined vapor cells have been previously proposed and demonstrated by use of a variety of innovative techniques, including wafer level glass blowing [4].

In many vapor cell applications, integrated optical reflectors are required for optical routing through the cell. Such designs are preferable for system integration and miniaturization because the light is returned to the plane of the source. This allows the optical source and detection elements to be located on the

same side of the cell. For example the Honeywell [5] chip scale atomic clock (CSAC), as described in [6], incorporates micromachined angled silicon reflectors within the physics package for routing laser light through the vapor cell from a vertical cavity surface emitting laser (VCSEL) to a coplanar photodiode. Even though simpler to implement than coated reflectors, bare silicon is an inefficient reflector at the required laser wavelengths for atomic clocks and sensors, yielding optical losses of nearly 70%.

As miniaturization of atomic systems progresses to compact systems for remote applications, the power available to operate these systems is restricted. For example, CSAC packages with power consumption below 200 mW have been demonstrated and a CSAC with consumption below 50 mW is targeted for remote applications requiring battery power [7]. In addition, elegant designs based on natural divergence of the VCSEL for sensor applications reduce the power available to the signal carrying component of the light [8,9]. Both the severe power budgets on the VCSEL and the increased functionality requested of the VCSEL require an improvement in the efficiency of the integrated reflectors.

\* Corresponding author. Tel.: +1 949 824 6314.

E-mail addresses: [max.perez@uci.edu](mailto:max.perez@uci.edu), [max.a.perez@gmail.com](mailto:max.a.perez@gmail.com) (M.A. Perez).

URL: <http://mems.eng.uci.edu> (M.A. Perez).

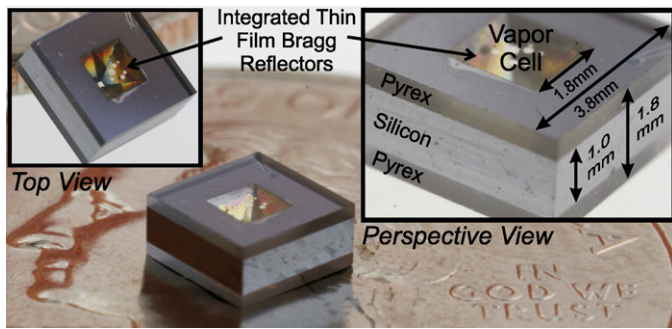


Fig. 1. Vapor cell with integrated multilayer thin film reflectors (on a US quarter for scale) with corresponding dimensions.

Previous devices incorporate deposited optical thin films to improve the reflective efficiency. A simple reflector may be formed by incorporating a metallic film, such as a copper reflector used in the vapor cell of the Symmetricom [5] CSAC [10]. Due to effects such as thermal currents, metallic reflectors within the vapor cell may disturb the sensitive electromagnetic environment required for many miniature vapor cell applications [11]. Metallic coatings are also vulnerable to oxidation and can react with alkali atoms, which can degrade their reflectivity over time. In addition, it may be difficult to control the polarization state of the reflected light using metallic reflectors. In this work, thin film dielectric structures are used to form reflectors which improve the reflector efficiency without the drawbacks imposed by metals.

This paper demonstrates a set of high efficiency nonmetallic multilayer thin film reflectors integrated into a micromachined rubidium vapor cell, shown in Fig. 1. This work is an expansion of the preliminary results presented at IEEE MEMS 2008 [12]. In Section 2, we explore the optical characteristics of bulk micromachined reflectors and demonstrate the need for improved reflectance characteristics through thin film structures, in particular in miniaturized atomic inertial sensors. The characteristics of the deposited angled Bragg reflectors are described in Section 3. In Section 4, the fabrication of the miniature vapor cell with integrated Bragg reflectors is described. In Section 5, the reflectors are characterized at the designed target wavelength, and the viability of the reflector containing miniature vapor cell is demonstrated. The implications of systematic nonuniformities due to the reflector fabrication technique are discussed in Section 6.

## 2. Design of micromachined reflectors

### 2.1. Integrated micro-reflectors for atomic MEMS

Many applications are emerging for micromachined atomic vapor cells as the central element for MEMS sensors based on nuclear or electron magnetic resonance (NMR). The complexity of these systems requires innovative micromachined components to achieve a compact miniaturized implementation. Traditionally, in order to achieve magnetic resonance in the vapor of an enclosed alkali metal, a two crossed beam approach is used [13]. This basic architecture has been the basis for a variety of magnetometers [14], as well as proposed for gyroscopes [15]. However, this approach generally requires multiple propagating beams from either external reflectors or optoelectronic components distributed around the vapor cell. Optical reflectors integrated directly into the vapor cell increase the potential for a compact miniaturized implementation by enabling a crossed beam architecture without additional assembled components.

A simplified NMR magnetometer has been demonstrated that reduces the optical source to a single diverging beam [8]. In this

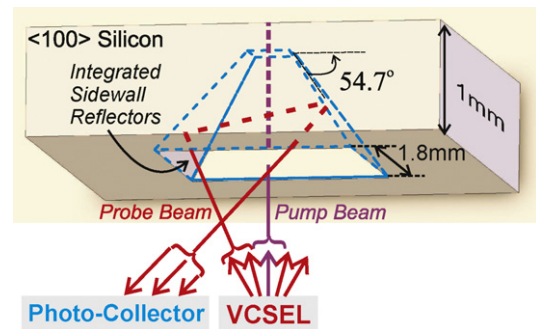


Fig. 2. Optical return cell with integrated sidewall reflectors for operation with a planar vertical cavity surface emitting laser (VCSEL) and photocollector elements.

implementation, the inner and outer beam components are used to form the respective pump and probe paths. Based on this diverging beam concept, an atomic MEMS NMR gyroscope has been proposed [9]. The optical design requires that the outer probe segment of the diverging beam from a VCSEL is reflected through the center of the miniature atomic vapor cell and returned to the plane of the source, while the central segment is used for optical pumping, as shown in Fig. 2. This geometry reduces the cell interrogation to a single plane of optoelectronic components while minimizing the possibility of optical feedback, which may result in undesirable effects such as mode-hopping in the VCSEL laser [16,17]. Optical feedback is more likely to occur in a vapor cell with a simple, non-angled backplane integrated reflector, such as in the Symmetricom [5] CSAC [10], where much of the incident power is directly returned to the optoelectronics plane and the VCSEL.

The demands of atomic MEMS applications require that integrated reflectors must be designed to preserve both the intensity and polarization state of the light at a specific optical wavelength to be effective. Vapor cells for NMR gyroscopes typically encapsulate gasses such as cesium or rubidium, which absorb circularly polarized light at specific optical absorption line wavelengths. The absorption of circularly polarized light is used for both the state preparation (pump) and detection (probe) of the alkali gas. For the system that we describe, the reflectors are designed for the  $D_1$  absorption line of  $^{87}\text{Rb}$  at a wavelength around  $\lambda \approx 795 \text{ nm}$ .

### 2.2. Silicon reflectors

Chemically etched angled silicon surfaces have long been reported to be applicable for redirecting optical beams ([18], for example). However, the reflective properties of an uncoated, bare silicon surface are poorly suited for the high-efficiency routing of light. The maximum reflection of general, unpolarized light from an ideal silicon surface may be calculated from the optical properties of bulk silicon. At an optical wavelength  $\lambda$  of 795 nm, the complex optical index of silicon is  $n + ki = 3.68 + 7 \times 10^{-3}i$ , where  $n$  is the index of refraction and  $k$  is the coefficient of extinction of the material. The reflectivity from the surface of a bulk material at normal incidence may be calculated as

$$R = \frac{(n-1)^2 + k^2}{(n+1)^2 + k^2}, \quad (1)$$

which for silicon yields a reflectivity of 0.33 [19]. This indicates that a maximum of 33% of the optical power will be reflected from a silicon surface, with the remaining power transmitted through or absorbed by the reflector material. For the reflection from two silicon surfaces, such as is required for return reflection,  $R_{\text{total}} = R^2 = 0.11$ . This indicates a loss of at least  $1 - R_{\text{total}} = 0.89 = 89\%$  from bulk transmission within a bare silicon return reflector cell, which is excessive and undesirable. For bulk silicon, both  $n$  and  $k$

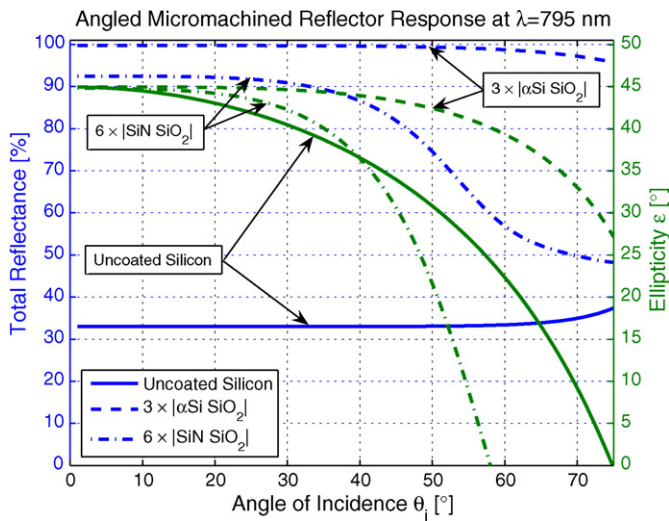


**Fig. 3.** Reflectance and ellipticity of micromachined reflectors under ideally incident circularly polarized light at  $\lambda = 795$  nm.

decrease as the wavelengths lengthen into the infrared with a corresponding decrease in reflectivity and increased need for reflective coatings.

In addition, bulk dielectric reflectors such as uncoated silicon have a limited capacity for maintaining circular polarization for reflection at non-normal angles of incidence. Light in a state of circular polarization has the optical power is equally divided between the plane parallel (p-polarized) TM and plane perpendicular (s-polarized) TE waves, which are out of phase with each other by  $\pi/2$ . Reflected light must maintain both the magnitude and phase conditions to remain circularly polarized. The difference between the TM and TE wave reflectance causes the state of polarization to become linearly polarized along the plane perpendicular direction. At increasing angle of incidence, the polarization ellipse becomes increasing linear until, at the Brewster's angle, reflected light becomes linearly polarized and circularly polarization characteristics are completely lost.

The state of polarization may be characterized by the ellipticity angle  $\epsilon$  of the light. At  $\epsilon = \pm 45^\circ$ , the light is ideally circularly polarized, while at  $\epsilon = 0^\circ$ , the light is linearly polarized [20]. Both the reflectance and ellipticity response of circularly polarized light reflected from uncoated silicon is shown in Fig. 3. The reflectance remains constant at 33% over a wide range of angles. However, the reflected ellipticity drops rapidly towards zero for angles greater than  $32^\circ$  making such a reflector unsuitable for applications requiring non-normal angles of incidence.

### 2.3. Dielectric multilayer reflectors

Multilayer structures of thin films of dielectric material may be used to increase the optical reflectivity. In the distributed Bragg reflector (DBR), light reflected at the interface between each layer is designed to constructively interfere to maximize the total reflected optical power at a specific wavelength. The reflectivity is maximized if the structure is composed of alternating layers of two materials of different indices of refractions. If the optical thickness of each layer is one-quarter wavelength of the light to be reflected, such that

$$t_{\text{layer}} = \frac{\lambda_c}{4n}, \quad (2)$$

where  $t_{\text{layer}}$  is the thickness of each layer,  $\lambda_c$  is the wavelength of light to be reflected and  $n$  is the index of refraction of each layer, the

reflectance at normal incidence of such a structure at  $\lambda_c$  is given by

$$R = \left( \frac{1 - (n_H/n_L)^{2p}(n_H^2/n_s)}{1 + (n_H/n_L)^{2p}(n_H^2/n_s)} \right)^2. \quad (3)$$

$n_H$  and  $n_L$  are the higher and lower index of refractions of each of the thin film materials, respectively,  $p$  is the number of layer pairs, and  $n_s$  is the index of refraction of the substrate [21]. The materials are assumed to be optically lossless ( $k = 0$ ). It can be readily seen that reflectivity increases rapidly for both an increasing optical index contrast ( $n_H/n_L$ ) and for an increasing number of layers.

A variety of dielectric materials are available for deposition onto silicon structures by use of conventional thin film techniques. Amorphous silicon ( $\alpha$ Si) provides a high index of refraction of  $n_H = 3.9$ , while silicon dioxide ( $\text{SiO}_2$ ) has a low index at  $n_L = 1.45$  at  $\lambda = 795$  nm [19]. Use of these materials yields a high optical index contrast ( $n_H/n_L = 2.7$ ). On a silicon substrate,  $p = 3$  layer pairs (six total layers) form a mirror of  $R = 0.997$ , or better than 99% efficiency after two reflections.

At lower infrared and visible wavelengths, the coefficient of extinction of amorphous silicon is small but not negligible, since at  $\lambda = 795$  nm,  $k_{\alpha\text{Si}} = 0.13$ . This may result in absorptive losses within the multilayer reflector [19]. Alternatively, silicon nitride (SiN) may be used as a high index material with  $n_H = 2.0$  and negligible absorptive loss at this wavelength ( $k_{\text{SiN}} < 2.2 \times 10^{-4}$ ) [19]. However, the contrast with silicon dioxide is reduced to  $n_H/n_L = 1.4$  and  $p = 6$  layer pairs or twelve total layers are required to reach a maximum individual mirror reflectance of  $R = 0.925$  (or equivalently 85% efficiency after two reflections). For both systems, the losses in the silicon dioxide used as the low index reflector material are negligible ( $k_{\text{SiO}_2} < 4.7 \times 10^{-6}$ ) [19].

In addition, ideal quarter wave Bragg reflectors are able to preserve circular polarization upon reflection at their design wavelength  $\lambda_c$ . As shown in Fig. 3, the twelve layer  $6 \times |\text{SiN SiO}_2|$  reflector will maintain the circular polarization to within  $5^\circ$  of ellipticity for incidences up to almost  $35^\circ$ , while the six layer  $3 \times |\alpha\text{Si SiO}_2|$  will maintain the same ellipticity for incident angles up to  $58^\circ$ .

### 3. Thin film deposition onto cavity sidewalls

Multilayer dielectric coatings for the formation of reflectors are generally formed by either physical vapor deposition (PVD) or chemical vapor deposition (CVD). PVD techniques, include sputtering or vacuum evaporation, are the traditional methods for depositing optical thin films for the formation of the dielectric reflectors. However, CVD techniques, especially plasma enhanced chemical vapor deposition (PECVD) has many practical advantages for formation of thin film reflectors, including higher deposition rates, continuous material flow allowing a large number of deposition steps under continuous vacuum and the formation of films with better robustness to environmental changes [22].

Commonly, PECVD process tools are designed and developed for use in coating planar substrates such as semiconductor wafers. PECVD is also frequently used for filling processes, such as into micromachined trenches and cavities. However, optical coatings deposited onto the surfaces of non-planar micromachined features are rarely reported. One notable exception is the proposed fabrication of optical structures onto surface etched facets as optical couplers for integrated optoelectronic devices [23]. However, the integration of multilayer Bragg reflectors onto surfaces inside deeply etched cavities, such as is necessary for the fabrication of micromachined vapor cells, has not been previously reported.

One difficulty with the fabrication of these reflectors is the nonuniformity of deposited films inside narrow features. Adams showed in 1983 that PECVD films deposited onto the sidewalls of narrow cavities are not uniform and decrease in thickness with

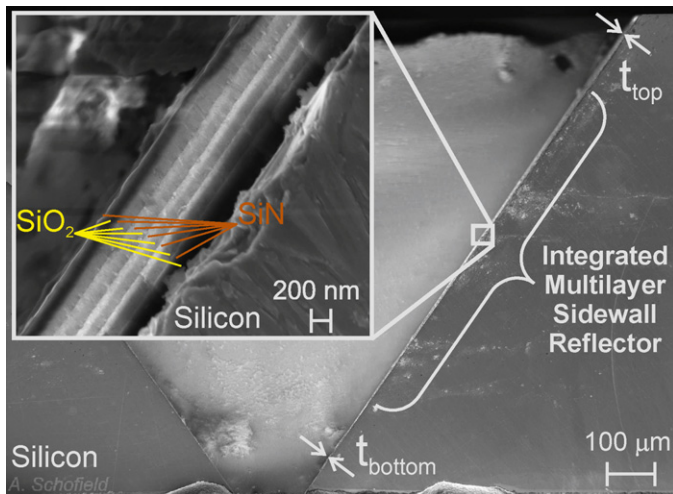


**Fig. 4.** Cross section of 12 alternating layers of silicon nitride and silicon oxide forming a thin film Bragg reflector deposited onto the angled (1 1 1) sidewalls of an etched silicon wafer (courtesy A. Schofield).

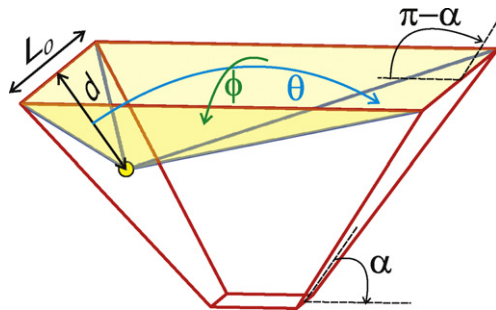


**Fig. 5.** Orthogonal arrival angles ( $\theta$ ,  $\phi$ ) for deposition along the sidewall centerline of a symmetric bulk micromachined cavity of wet etch angle  $\alpha$  and square etch window of edge length  $L_0$ .

depth [24]. These variations are attributed to the high mean free path of the low pressure vapor species during deposition and insufficient reactant species migration along the surface. This results in a thin film deposition rate that depends strongly on the arrival angles open to the PECVD reactor.

Adams demonstrated how a proportionality between the arrival angle in a cross section of a vertical trench and the PECVD rate accounts for the nonuniformity of a PECVD film deposited onto the sidewalls of etched vertical cavities. The notable difference in the total thickness of a 12-layer sidewall integrated silicon nitride Bragg reflector between the top ( $t_{\text{top}}$ ) and bottom ( $t_{\text{bottom}}$ ) of the etched cell shown in Fig. 4 illustrates this effect on the total thickness of a Bragg reflector.

Adams' model may be extended to describe the deposition onto anisotropically etched angled sidewalls as the product of the two orthogonal sidewall arrival angles. Fig. 5 shows the two orthogonal

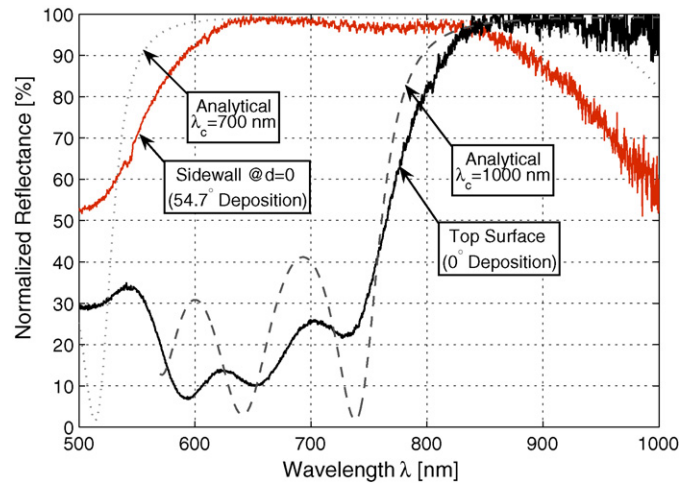


**Fig. 6.** Shift in normalized reflector spectrum as deposited perpendicularly on cell top planar surface ( $0^\circ$ ) and on angled sidewall surface near the top of the cell ( $\alpha = 54.7^\circ$ ) in a  $6 \times |\alpha\text{Si SiO}_2|$  Bragg reflector.

arrival angles both between the deposition face and the opposite wall ( $\theta$ ) and between the two adjacent walls ( $\phi$ ). The deposition face has a wet etch angle  $\alpha$ . Arrival angle  $\theta$  may be calculated by

$$\theta = \sin^{-1} \left\{ \sqrt{\frac{L_0^2 \sin^2(\alpha)}{L_0^2 + d^2 - 2L_0d \cos(\alpha)}} \right\}, \quad (4)$$

where  $d$  is the depth along the sidewall face,  $L_0$  is the cavity opening width,  $\alpha$  is the etch angle, and the oblique or acute angle solution for  $\sin^{-1}\{\cdot\}$  must be chosen to provide the physically suitable and continuous solution as a function of sidewall depth. Arrival angle  $\phi$  is calculated by

$$\phi = 2 \tan^{-1} \left\{ \frac{L_0}{2d} \right\}, \quad (5)$$

which for  $L_0/d \ll 1$  is the same as the approximate  $\phi = \tan^{-1}\{L_0/d\}$  deposition thickness dependence presented by Adams for vertical sidewalls.

The dependence of the PECVD deposition rate on the arrival angles at the cavity sidewalls may be used to account for two optical characteristics observed in the multilayer reflectors fabricated in this work, including a discrete step reduction in the high reflectance wavelength band between the top surface to the angled sidewall and a continuous reduction in the high reflectance wavelength band down the cavity sidewall. These characteristics were observed in Bragg reflectors composed of two different material systems deposited on the angled sidewalls of identical cavity geometries. Two different commercial PECVD tools are used to form angled Bragg reflectors formed of three pairs of alternating amorphous silicon and silicon dioxide ( $3 \times |\alpha\text{Si SiO}_2|$ ) and six pairs of alternating silicon nitride and silicon dioxide ( $6 \times |\text{SiN SiO}_2|$ ) thin film struc-

**Table 1**  
Thin film PECVD of cavity sidewall Bragg reflectors.

Film	Deposition parameters			Gas flow rates [sccm]				
	$T$ [ $^\circ\text{C}$ ]	Pressure [mTorr]	Power [W]	$\text{N}_2$	$\text{N}_2\text{O}$	$\text{SiH}_4$	$\text{O}_2$	Ar
PlasmaTherm 790 PECVD ( $3 \times  \alpha\text{Si SiO}_2 $ )								
$\text{SiO}_2$	250	900	25	150	50	2.75	–	–
$\alpha\text{Si}$	250	980	30	75	4	–	–	–
BMR ICP PECVD ( $6 \times  \text{SiN SiO}_2 $ )								
$\text{SiO}_2$	300	5	1000	–	–	9.6	18	20
$\text{SiN}$	300	5	1000	17.5	–	20	–	20

**Table 2**

Comparison between arrival angle geometry and reflector wavelength with deposition type for a  $6 \times |\alpha\text{Si SiO}_2|$  reflector from Fig. 6.

Deposition type	Arrival angles			$\lambda_c$ [nm]
	$\theta$ [rad]	$\phi$ [rad]	$\theta \times \phi$ [rad <sup>2</sup> ]	
Planar	$\pi$	$\pi$	$\pi^2$	$1000 \pm 50$
Sidewall (at $d = 0$ )	$\pi - \frac{54.7^\circ}{180^\circ} \pi$	$\pi$	$\pi \left( \pi - \frac{54.7^\circ}{180^\circ} \pi \right)$	$700 \pm 50$
Sidewall/planar	0.7	1.0	0.7	$0.7 \pm 0.1$

tures under continuous vacuum using the parameters shown in Table 1.

The optical response was nondestructively characterized using the normalized broadband reflection spectrum of the sidewall reflectors sampled over a nominal spot size of  $200 \mu\text{m}$  with a surface reflection probe (Ocean Optics R200-7-VIS-NIR [5]) coupled to a halogen light source (Ocean Optics LS-1 [5]). Although the variation in film thickness down the cavity sidewall could be directly observed in SEM micrographs (as shown in Fig. 4), variation in the reflectance spectrum proved more reliable in characterizing the effects due to cavity sidewall deposition.

### 3.1. Step shift

A step reduction in deposition rate from normal deposition on the top, outside surface to the angled sidewall results from the abrupt reduction in arrival angle from the outside surface to the angled sidewall. The reduction in deposition rate results in a discrete shift in the standard, planar film deposition rate for any given PECVD system. This shifts the reflectance characteristics to lower wavelengths in proportion to the decrease in deposition rate, as expected from (2) and shown in Fig. 6. The center wavelength  $\lambda_c$  is estimated from the experimental reflectance spectrum by comparison with the analytical calculation of the reflectance spectrum.

Table 2 shows the arrival angles at the surface and the top ( $d = 0$ ) of the angled sidewall and their product compared to the center wavelengths from Fig. 6. The ratio of the product of the arrival angles and the ratio of center, design wavelengths  $\lambda_c$  between the multilayer reflector deposited on the top planar surface and angled sidewall are observed to be identical to within 15% error. This correlation suggests that the ratio of arrival angle products predicted from the cavity geometry may be used to estimate the shift in reflectance band for a Bragg reflector deposited onto a cav-

ity sidewall. For deposition onto the inner sidewall of a cavity of the examined geometry with a  $54.7^\circ$  etch angle, the change in arrival angle suggests a 30% reduction in deposition rate and reflector wavelength from planar to sidewall deposition.

### 3.2. Continuous shift

The continuous reduction in the arrival angle progressing into the cavity results in a continuous thinning of the thin film deposited down the sidewall of the cavity. This results in a color gradient that is clearly evident to the naked eye, as shown in the top view insert to Fig. 1. This gradient progresses along the sidewall reflector from the top of the vapor cell to the bottom and shows a shift from red to blue. This indicates a shift in the wavelength  $\lambda$  at which the mirror has maximum reflectance from the longer red wavelengths to shorter wavelengths of maximum reflectance in the blue. The shift in the reflectance band of the sidewall reflectors is greater than 400 nm over a length of less than  $600 \mu\text{m}$  down the sidewall centerline, as shown in Fig. 7. This downward shift in reflector wavelength is accompanied by a reduction in reflector bandwidth, as expected when characterized in (un-normalized) wavelength units [21].

The center wavelength  $\lambda_c$  may be estimated from the wavelength at maximum reflectance  $\lambda_{R_{\text{max}}}$ , which is extracted directly from the reflectance characterization in Fig. 7. As expected from (2), this characteristic wavelength is proportional to the sidewall deposition rate. Over the characterization distance on the upper half of the sidewall reflector, a decrease in deposition rate of more than 40% is observed, as shown in Fig. 8. When the variation in  $\lambda_{R_{\text{max}}}$  down the sidewall is compared to the variation in the arrival angles, it is observed that the product of the arrival angles  $\theta \times \phi$  correlates well with the variation in  $\lambda_{R_{\text{max}}}$ . This suggests that the sidewall deposition rate can be well characterized by the arrival angle product, as is expected from the dependence on the solid arrival angle suggested by Adams.

Due to the continuous variation in deposition rate on the cavity sidewalls and subsequent shift in reflector wavelength, it is challenging to maintain high reflection at a single wavelength over the entire sidewall. However, by forming a Bragg reflector with a wide reflection bandwidth, the reflection at the target wavelength may be maximized over as much of the sidewall as possible. The reflection band is maximized by choosing thin films with a high optical contrast, such as is evident in the larger bandwidth of the  $|\alpha\text{Si SiO}_2|$  reflector (Fig. 7(a)) relative to that of the  $|\text{SiN SiO}_2|$  reflector (Fig. 7(b)).

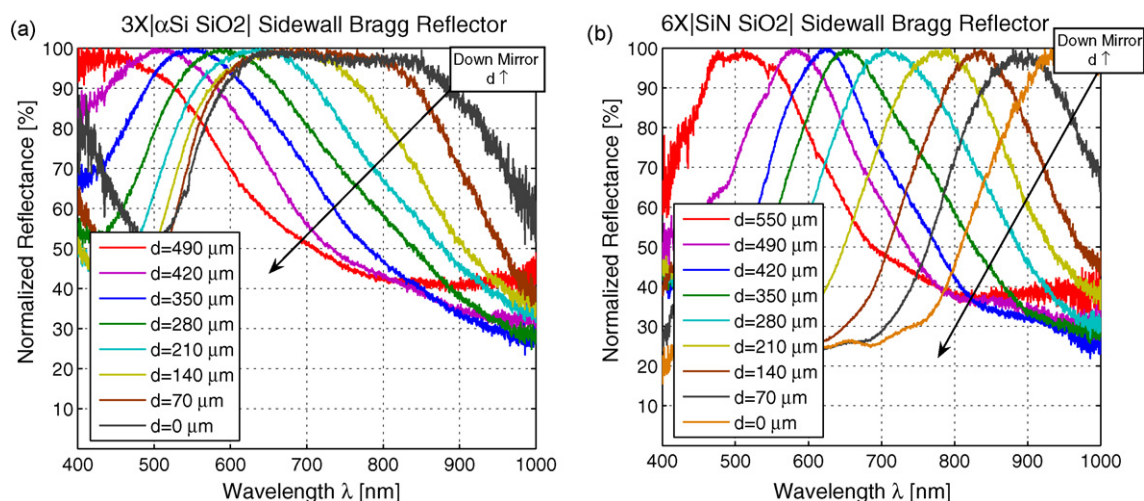


**Fig. 7.** Normalized reflectance shift in sidewall integrated Bragg reflector with vertical position  $d$  down the cavity sidewall. (a)  $3 \times |\alpha\text{Si SiO}_2|$  sidewall reflector. (b)  $6 \times |\text{SiN SiO}_2|$  sidewall reflector.

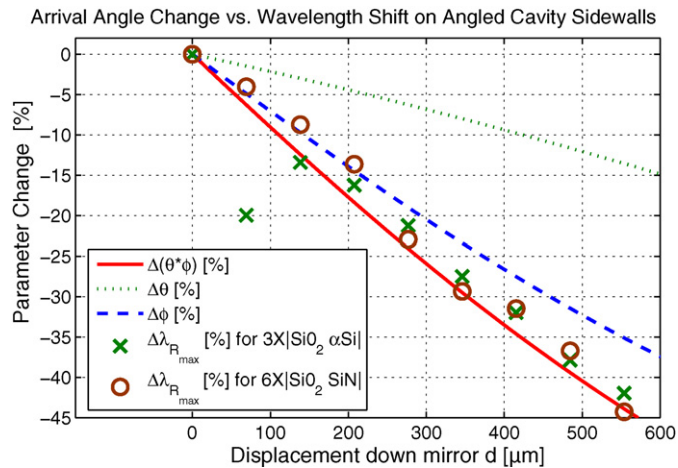


**Fig. 8.** Change in arrival angles ( $\Delta\theta$ ,  $\Delta\phi$ ,  $\Delta(\theta \times \phi)$ ) and the experimentally measured change in wavelength of maximum reflectance ( $\Delta\lambda_{R_{max}}$ ) from Fig. 7.

To minimize the effects due to the shifting reflector and because of the wider available reflector bandwidth, the completed vapor cell was formed from a cavity with an integrated six layer  $3 \times |\alpha\text{Si SiO}_2|$  Bragg reflector. This choice in the reflector design increases the reflector bandwidth at the expense of having slightly higher absorption over the SiN based reflectors. However, high reflectance is maintained over larger variation in the total Bragg reflector thickness and, thus, over a larger surface area of the cell cavity sidewalls.

#### 4. Vapor cell fabrication

The fabrication of the cell is a hybrid of traditional wet etch bulk micromachining [25], optical thin film deposition [22], and anodic wafer bonding [26]. Referring to Fig. 9, the first three steps are of an anisotropic silicon wet through-etch. The next four steps are the processing related to the optical films. The final step is the encapsulation of alkali vapor and buffer gasses.

In Step 1, we start with a 1 mm thick double side polished (DSP) undoped silicon wafer. On each side of the wafer, a 3000 Å thick silicon nitride layer is deposited via low pressure chemical vapor deposition (LPCVD). The silicon nitride is used as a wet etch hardmask. In Step 2, a 1.8 mm sided square is patterned lithographically

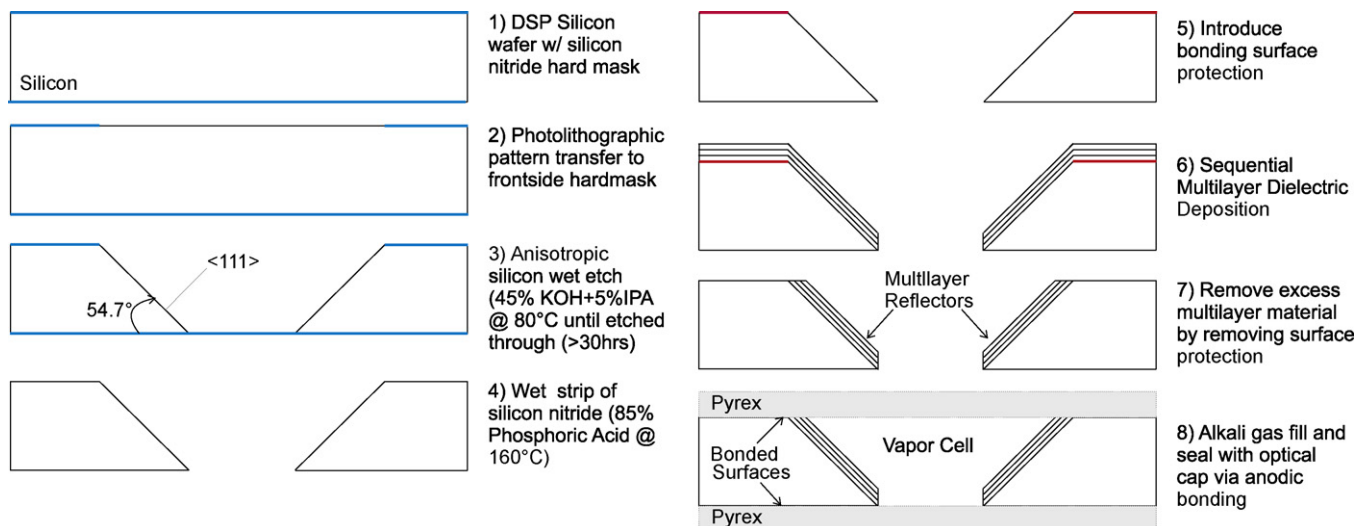


**Fig. 9.** Fabrication of the bulk micromachined silicon reflector preform with the high reflectance multilayer sidewall reflector, including the final anodic bonding and gas encapsulation process.

**Table 3**  
Return reflection vapor cell characteristics.

Reflector cell		Vapor cell		Multilayer reflector	
Optical element	Dimension	Gas	Pressure [Torr]	Thin film	$t_{\text{layer}}$ [nm]
Reflector area (4×)	1.3 mm <sup>2</sup>	<sup>87</sup> Rb	condensed	$\alpha\text{Si}$ (3×)	60
Reflector angle	54.7°	Xe	153	$\text{SiO}_2$ (3×)	140
Cell window	3.2 mm <sup>2</sup>	N <sub>2</sub>	1100		
Cell volume	1 mm <sup>3</sup>				

by use of a AZ4620 photoresist mask. This mask is aligned to the  $\langle 100 \rangle$  wafer flat. The cell window pattern is transferred to the silicon nitride hardmask via a short reactive ion etch (RIE). In Step 3, the patterned wafer is immersed in a bath of 45% (by volume with water) potassium hydroxide (KOH) to which is added 5% (by volume) isopropyl alcohol (IPA). The bath is heated to 80 °C, causing the exposed silicon to etch at  $\sim 0.5 \mu\text{m}/\text{min}$ , revealing the surfaces of the  $\langle 111 \rangle$  crystalline planes. This forms a cell with flat, angled sidewalls inclined at 54.7° to the wafer surface. The etch is allowed to progress through the wafer, typically taking more than 30 h.

In Step 4, the silicon nitride hardmask is chemically removed via a hot 160 °C phosphoric acid dip. In Step 5, the top surface of the etched silicon is stamped onto a shallow photoresist film and allowed to dry, which provides protection to the anodic bonding surfaces during subsequent deposition. Then in Step 6, the  $3 \times |\alpha\text{Si SiO}_2|$  optical films are sequentially deposited by PECVD using the PlasmaTherm 790 parameters described in Table 1 under a continuous vacuum. In Step 7, the final cell preform is fabricated by removing the top surface protection via a fuming sulfuric acid dip, resulting in the lift-off of the excess thin film material and cleaning of the surfaces.

In Step 8, the preform is filled with the alkali material using the technique described previously in [27]. In brief, the filling method consists of combining BaN<sub>6</sub> and <sup>87</sup>RbCl inside a glass ampoule. The ampoule nozzle is aligned to the cell preform within a vacuum chamber and heated to release <sup>87</sup>Rb into the cell preform. Then buffer gasses are admitted into the chamber and the cell is sealed via anodic bonding between two transparent Pyrex 7740 [5] plates. In this case, the vapor cell was filled with <sup>87</sup>Rb along with buffer gasses of 153 Torr Xe and 1100 Torr N<sub>2</sub>. The top plate forms a window that allows optical access to the vapor. The characteristics of the fabricated vapor cell are tabulated in Table 3.

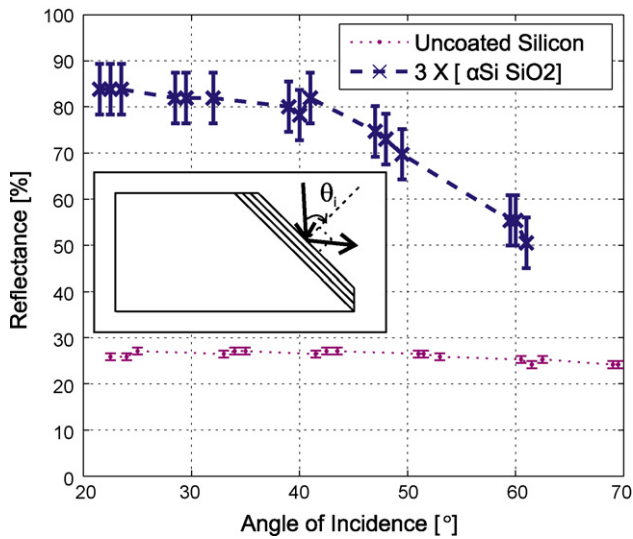


Fig. 10. Reflectance from a single bulk micromachined silicon sidewall reflector with and without multilayer reflectors.

### 5. Characterization

#### 5.1. Cavity sidewall reflector

The reflection of an individual etched sidewall was characterized by splitting a cell (after Step 7 of fabrication) and mounting the cleaved face on a rotation stage. In this experiment, we used a single mode VCSEL temperature stabilized at 20 °C using a commercial laser diode mount (Thorlabs TCLDM9 [5]). The light beam from the VCSEL was directed at the surface and was focused using an aspheric lens to spot size at the sample of less than a 0.25 mm in diameter across less than 20% of the surface (down cavity) length and less than 4% of the surface area of the cavity sidewall. The reflected beam was collected and the power monitored by a photodiode at different reflection angles of incidence. Fig. 10 shows the power collected normalized by the VCSEL emission power. The reflective surfaces of the cell are characterized to have a reflectance over 80% for incident angles up to 40°, which is almost three times greater than that of an identically etched bare silicon sidewall reflector, which exhibits a reflectance under the same experimental conditions of less than 30%. Up to 6.2% loss may be attributed to optical absorption in the reflector itself [28], while the remaining deviation from ideal reflectance likely due to the characterized thin film nonuniformity. In addition, the experimentally observed angle of incidence limitation in excess of that expected from Fig. 3 is also likely due to the shifting thin film thickness.

#### 5.2. Vapor cell

To characterize the optical absorption by the encapsulated vapor, the light from the VCSEL was passed directly through the complete vapor cell, shown in Fig. 1. A small resistive heater was used to elevate the cell temperature, increasing the vapor pressure of the <sup>87</sup>Rb within the enclosed cell. The emission wavelength of the VCSEL was swept by varying the drive current at constant VCSEL temperature from approximately 794.5 nm at 1.0 mA to 795.1 nm at 2.0 mA estimated from the published response characteristics of the VCSEL [29]. At increased vapor pressure under elevated temperatures, wavelength swept VCSEL light transmitted through the cell showed significant absorption at the D<sub>1</sub> atomic transition of <sup>87</sup>Rb (794.8 nm in air), demonstrating alkali vapor encapsulation (Fig. 11).

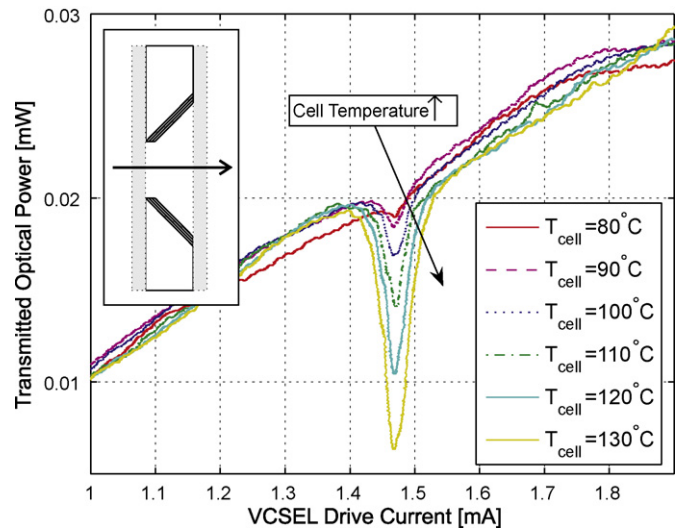


Fig. 11. Optical absorption of the <sup>87</sup>Rb D<sub>1</sub> atomic transition in the vapor cell under elevated temperature (*T<sub>cell</sub>*) versus VCSEL drive current (laser frequency).

#### 5.3. Return reflection

The VCSEL beam was then directed onto one sidewall of the cell. The beam was reflected through the cell and redirected back towards the plane of emission for detection by the reflector on the opposite sidewall. The temperature of the cell was held fixed at a temperature of 100 °C by use of feedback control, and the VCSEL drive current was tuned until a pronounced absorption peak was detected indicating vapor cell interrogation under return reflected light (Fig. 12). Although the Bragg reflector bandwidth will shift to longer wavelengths at elevated temperature, since the thermal expansion coefficient of both amorphous silicon and silicon dioxide is less than  $3 \times 10^{-6}/^{\circ}\text{C}$  around room temperature, temperature change of less than 100 °C, will result in shifts in the reflector bandwidth of less than 0.03%. When normalized by the optical power of the source, under a return reflective path, an optical efficiency of 40% for the reflector cell was demonstrated. This is four times better than the 10% return reflection efficiency from a similarly etched silicon cell preform.

Not included in the efficiency of the bare silicon preform are losses additional to reflector inefficiencies in the complete vapor

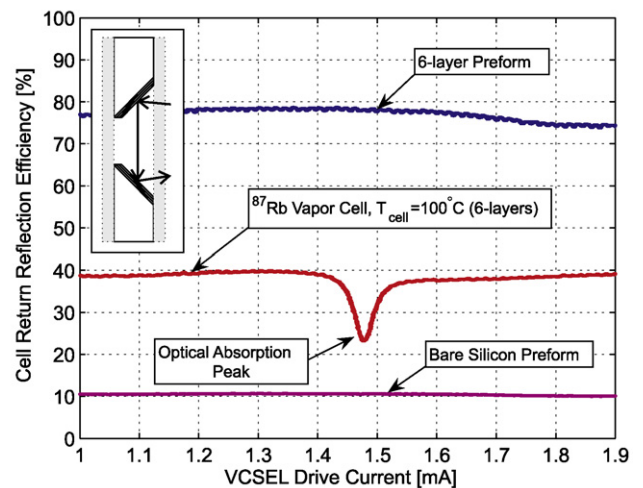


Fig. 12. Optical efficiency of the vapor cell and cell preforms during return reflection with and without integrated reflectors.

cell. Nominally, a 4% reflective losses at each glass interface is expected yielding an estimated 16% total loss from the cap window for the double cell sidewall reflection path. An optical efficiency approaching 78% was observed in a preform incorporating thin film reflectors fabricated side-by-side with the complete vapor cell. The 22% difference between the complete vapor cell and unfilled preform might be associated with scattering due to an abundance of rubidium observed to be condensed on the cell window. An additional loss source might be the deposition of some portion of the rubidium precursors, resulting from an incomplete reaction between the barium azide and the rubidium chloride, on the reflector surfaces and contributing to the observed absorption losses. However, comparison between the two unfilled preforms, with and without thin film reflectors, indicate that the multilayer reflectors improve the optical efficiency by a factor of seven to eight for an optical path with two reflections.

## 6. Discussion

Although the optical performance of the cell with dielectric reflectors is increased dramatically over that expected from a vapor cell formed from uncoated silicon, the performance is less than might be expected from the analytical estimates according to (3). It is expected that this is due to the variations in the thin film thickness from the optical optimum thickness expressed by (2), as explored in Section 3. Although it has been demonstrated here that the characteristics of PECVD for the fabrication of Bragg reflectors in vapor cell geometries will result in a strong variation in the reflected wavelength with reflector position, these variations may be predicted by the cavity geometry. Due to this predictability, the decrease in reflectance performance may be mitigated by an optical thin film design optimized to accommodate this variation. Thin film designs optimized for integrated sidewall reflectors with deposition nonuniformity are outside the scope of this paper.

More advanced thin film reflector designs have been proposed to generate specific polarization states upon reflection. Of specific interest to atomic MEMS applications are thin film phase shifting reflectors, which may be used to generate circularly polarized light from the VCSEL light eliminating the need for the generally required phase retarding quarter wave plate [30]. However, advanced designs with additional polarization functionality useful for atomic MEMS would be difficult to achieve under such film nonuniformity. However, such designs may be implementable under fabrication conditions optimized for sidewall film uniformity. Using PVD processes, which proceed under lower pressures resulting in line-of-sight deposition, it may be possible to minimize cavity sidewall deposition nonuniformities. Emerging techniques, such as atomic layer deposition (ALD), that are both highly conformal and uniform would be likely be suitable for the formation of highly uniform sidewall integrated Bragg reflectors [31,32]. However, the practical advantages of PECVD over these techniques would have to be sacrificed. Alternatively, the performance challenges due to nonuniform deposition using PECVD may be partially compensated for using advanced designs. An extended bandwidth reflector design has been demonstrated to provide high reflectance at the target wavelength over most of the cavity sidewall even under such nonuniform deposition conditions [33].

## 7. Conclusions

The use of multilayer thin film Bragg reflectors deposited on the sidewall of a bulk micromachined cell for integrated optics in vapor cells, as may be used for atomic MEMS sensors, has been demonstrated. In spite of process imperfections due to nonuniform deposition on angled surfaces, the multilayer reflectance is shown to be almost three times better than that of uncoated silicon. Under

the two reflections within a micromachined cell required for return reflection, the optical efficiency was observed to be improved by as much as eight times by integrating Bragg reflectors. A process suitable for the fabrication of encapsulated rubidium vapor cells containing integrated reflectors is demonstrated. The  $D_1$  absorption line of  $^{87}\text{Rb}$  is resolved in a miniaturized vapor cell by use of two integrated thin film reflectors with a return reflection efficiency near 40%.

## Acknowledgements

The authors thank the staff of the Integrated Nanosystems Research Facility (INRF) for fabrication support and A. Schofield for micrograph assistance in the Zeiss Center of Excellence. Numerical optical calculations were done using the ewa MATLAB<sup>®</sup> [5] package by S.J. Orfanidis. This work was supported in part by the Defense Advanced Research Projects Agency (DARPA) Navigation-Grade Integrated Micro Gyroscopes (NGIMG) program and is a partial contribution of the National Institute of Standards and Technology (NIST), an agency of the US government, and is not subject to copyright.

## References

- [1] L.-A. Liew, S. Knappe, J. Moreland, H. Robinson, L. Hollberg, J. Kitching, Microfabricated alkali atom vapor cells, *Appl. Phys. Lett.* 84 (2004) 2694.
- [2] S. Knappe, V. Shah, P.D.D. Schwindt, L. Hollberg, J. Kitching, L.-A. Liew, J. Moreland, A microfabricated atomic clock, *Appl. Phys. Lett.* 85 (9) (2004) 1460–1462.
- [3] P.D.D. Schwindt, S. Knappe, V. Shah, L. Hollberg, J. Kitching, L.-A. Liew, J. Moreland, Chip-scale atomic magnetometer, *Appl. Phys. Lett.* 85 (26) (2004) 6409–6411.
- [4] J.E. Eklund, A.M. Shkel, S. Knappe, E. Donley, J. Kitching, Glass-blown spherical microcells for chip-scale atomic devices, *Sens. Actuators A: Phys.* 143 (May (1)) (2008) 175–180.
- [5] Products, or companies named here are cited only in the interested of complete scientific description, and neither constitute nor imply endorsement by NIST or by the US government.
- [6] D.W. Younger, L.M. Lust, D.R. Carlson, S.T. Lu, L.J. Forner, H.M. Chanhvongsak, T.D. Stark, A manufacturable chip-scale atomic clock, in: *Transducers'07 & Eurosensors XXI: The 14th International Conference on Solid-State Sensors and Actuators and Microsystems*, June 2007.
- [7] S. Knappe, P.D.D. Schwindt, V. Gerginov, V. Shah, L. Liew, J. Moreland, H.G. Robinson, L. Hollberg, J. Kitching, Microfabricated atomic clocks and magnetometers, *J. Opt. A: Pure Appl. Opt.* 8 (7) (2006) S318–S322.
- [8] E. Hodby, E.A. Donley, J. Kitching, Differential atomic magnetometry based on a diverging laser beam, *Appl. Phys. Lett.* 91 (1) (2007) 011109.
- [9] J. Kitching, E. Donley, E. Hodby, A.M. Shkel, and E.J. Eklund, Compact atomic magnetometer and gyroscope based on a diverging laser beam (UC OTA Case # 2008–002), 2008.
- [10] R. Lutwak, J. Deng, W. Riley, M. Varghese, J. Leblanc, G. Tepolt, M. Mescher, D.K. Serkland, K.M. Geib, G.M. Peake, The chip-scale atomic clock low-power physics package, in: *36th Annual Precise Time and Time Interval Systems and Applications Meeting Proceedings*, 2004.
- [11] J. Nenonen, J. Montonen, T. Katila, Thermal noise in biomagnetic measurements, *Rev. Sci. Instrum.* 67 (6) (1996) 2397–2405.
- [12] M.A. Perez, U. Nguyen, S. Knappe, E. Donley, J. Kitching, A.M. Shkel, Rubidium vapor cell with integrated nonmetallic multilayer reflectors, in: *IEEE 21st International Conference on Micro Electro Mechanical Systems*, 2008 (MEMS 2008), January 13–17, 2008, pp. 790–793.
- [13] W.E. Bell, A.L. Bloom, Optical detection of magnetic resonance in alkali metal vapor, *Phys. Rev.* 107 (September (6)) (1957) 1559–1565.
- [14] D. Budker, M. Romalis, Optical magnetometry, *Nat. Phys.* 3 (April (4)) (2007) 227–234.
- [15] B.C. Grover, E. Kanegsberg, J.G. Mark, R.L. Meyer, Nuclear magnetic resonance gyro, US Patent 4,157,495, June 1979.
- [16] Y.C. Chung, Y.H. Lee, Spectral characteristics of vertical-cavity surface-emitting lasers with external optical feedback, *Photonics Technology Letters*, IEEE 3 (July (7)) (1991) 597–599.
- [17] M. Sciamanna, K. Panajotov, H. Thienpont, I. Veretennicoff, P. Mégret, M. Blondel, Optical feedback induces polarization mode hopping in vertical-cavity surface-emitting lasers, *Opt. Lett.* 28 (17) (2003) 1543–1545.
- [18] D.J. Sadler, M.J. Garter, C.H. Ahn, S. Koh, A.L. Cook, Optical reflectivity of micro-machined 111-oriented silicon mirrors for optical input–output couplers, *J. Micromech. Microeng.* 7 (December) (1997) 263.
- [19] E.D. Palik, *Handbook of Optical Constants of Solids*, vol. 1, Elsevier, 1998.
- [20] H.G. Tompkins, E.A. Irene, *Handbook of Ellipsometry*, William Andrew Publishing, Noyes, 2005.
- [21] H.A. Macleod, *Thin-Film Optical Filters*, 3rd ed., Institute of Physics Publishing, Bristol/Philadelphia, 2001.

- [22] L. Martinu, D. Poitras, Plasma deposition of optical films and coatings: a review, *J. Vac. Sci. Technol. A: Vac. Surf. Films* 18 (6) (2000) 2619–2645.
- [23] V. Gottschalch, R. Schmidt, B. Rheinlanderand, D. Pudis, S. Hardt, J. Kvietkova, G. Wagner, R. Franzheld, Plasma-enhanced chemical vapor deposition of SiOx/SiNx Bragg reflectors, *Thin Solid Films* 416 (September (1/2)) (2002) 224–232.
- [24] A.C. Adams, Plasma deposition of inorganic films, *Solid State Technol.* 26 (April 4) (1983) 135–139.
- [25] G.T.A. Kovacs, N.I. Maluf, K.E. Petersen, Bulk micromachining of silicon, *Proc. IEEE* 86 (August (8)) (1998) 1536–1551.
- [26] M.A. Schmidt, Wafer-to-wafer bonding for microstructure formation, *Proc. IEEE* 86 (8) (1998) 1575–1585.
- [27] S. Knappe, V. Gerginov, P.D.D. Schwindt, V. Shah, H.G. Robinson, L. Hollberg, J. Kitching, Atomic vapor cells for chip-scale atomic clocks with improved long-term frequency stability, *Opt. Lett.* 30 (2005) 351–2353.
- [28] D.I. Babic, S.W. Corzine, Analytic expressions for the reflection delay, penetration depth, and absorbance of quarter-wave dielectric mirrors, *IEEE J. Quantum Electron.* 28 (February (2)) (1992) 514–524.
- [29] ULM Photonics, Specification for single mode VCSEL 795 ± 3 nm TO46 & TEC. Technical report, ULM Photonics.
- [30] W.H. Southwell, Multilayer coating design achieving a broadband 90 degree phase shift, *Appl. Opt.* 19 (1980) 2688.
- [31] M. Ritala, M. Leskel, J.-P. Dekker, C. Mutsaers, P.J. Soininen, J. Skarp, Perfectly conformal tin and Al<sub>2</sub>O<sub>3</sub> films deposited by atomic layer deposition, *Chem. Vapor Depos.* 5 (1) (1999) 7–9.
- [32] M.K. Tripp, F. Fabreguette, C.F. Herrmann, S.M. George, V.M. Bright, Multilayer coating method for X-ray reflectivity enhancement of polysilicon micro-mirrors at 1.54- $\lambda$ -ring] wavelength, in: E.G. Johnson, G.P. Nordin, T.J. Suleski (Eds.), *Proceedings of the SPIE*, vol. 5720, SPIE, 2005, pp. 241–251.
- [33] M.A. Perez, J. Kitching, A.M. Shkel, Design and demonstration of PECVD multilayer dielectric mirrors optimized for micromachined cavity angled sidewalls, *Sens. Actuators A: Phys.* (2008), doi:10.1016/j.sna.2008.10.007, in press.

## Biographies



**Maximilian A. Perez** received his BS in Mechanical Engineering and in Material Science and Engineering from the University of California at Berkeley in 2002, his MS in Mechanical and Aerospace Engineering from the University of California at Irvine in 2004, and his PhD degree in Mechanical and Aerospace Engineering from the University of California at Irvine in 2008 focused on novel methods in optical and atomic inertial sensors. He has worked in the past at the Lawrence Berkeley Laboratory, the UC Berkeley Human Robotics Laboratory, and NASA's Jet Propulsion Laboratory. Mr. Perez's awards include the IEEE Sensors Council Graduate Student Scholarship Award (2006), 2nd Best Student Paper IEEE Sensor Conference (2006), 2nd Henry Samueli School of Engineering Annual Research Review (2003), the NSF Fellowship Honorable Mention (2002), the Elaine C. Shen Memorial Prize in Material Science and Engineering (2001) and was a National Merit Scholarship Commended Student (1997). Dr. Perez has published five refereed journal papers, ten conference papers and is currently employed by VIP Sensors in San Juan Capistrano, California.



**Uyen H. H. Nguyen** received her BS degree in electrical engineering and computer science at University of California, Berkeley in December 2008. Since then, she has been working as an EDA software engineer at Denali Software, Inc. in Sunnyvale, California.



**Dr. Svenja Knappe** received her diploma in physics in 1998, with a thesis on the investigation of single cesium atoms in a magneto-optical trap, and her PhD degree in 2001, on "Dark resonance magnetometers and atomic clocks" from the University of Bonn, Germany. Since 2001, she has been doing research with the Time and Frequency Division at the National Institute of Standards and Technology (NIST). Her current research is focused on the miniaturization of atomic sensors. In the past she worked on precision laser spectroscopy and laser cooling and trapping of atoms. She and her team developed the first microfabricated atomic vapor cells and laser wavelength stabilization, as well as chip-scale atomic clock and magnetometer physics packages at NIST. She has published more than 30 papers in refereed journals.



**Dr. Elizabeth Donley** is a member of the Atomic Devices and Instruments Group in the Time and Frequency Division of the National Institute of Standards and Technology. She received her BS in physics from University of Nevada, Las Vegas in 1994 and a MS in physics from the University of Colorado in Boulder in 1996. She got her PhD in natural sciences from the Swiss Federal Institute of Technology in Zürich in 2000. Her thesis research was on single-molecule spectroscopy at subkelvin temperatures. From 2000 to 2002 she was a postdoctoral fellow at JILA/The University of Colorado where she worked on Bose-Einstein Condensation. Since 2002, she has been a physicist in the Time and Frequency Division at NIST where she has worked on the operation and development of atomic fountain clocks and on various chip-scale atomic devices and instruments. Awards that she has received include the Department of Commerce Gold Medal and the Silver Medal Thesis Prize of the ETH Zürich.



**Dr. John Kitching** is the leader of the Atomic Devices and Instruments Group at the National Institute of Standards and Technology. He received his BSc in physics from McGill University in 1990. He went on to obtain a MSc and PhD in applied physics from the California Institute of Technology in 1992 and 1995, respectively. His thesis topic was an investigation of amplitude and frequency noise properties of semiconductor lasers subjected to optical feedback. From 1995 to 2003, he was with JILA/The University of Colorado and also held a guest-researcher appointment in the Time and Frequency Division at the National Institute of Standards and Technology, NIST. Since 2003, he has been a physicist in the Time and Frequency Division at NIST. His research interests include atomic clocks and frequency standards, quantum interference effects in atomic systems, and applications of semiconductor lasers to problems in atomic physics and frequency control. Most recently, he and his team pioneered the development of microfabricated atomic devices based on room-temperature alkali vapors for use as frequency references, magnetometers and other sensors. He has received several awards including the 2005 EFTF European Young Scientist Award, the 2006 ISSCC Jack Raper Award for Outstanding Technology Directions and the Department of Commerce Silver Medal. He has published over 50 papers in refereed journals, has given numerous invited talks and has been awarded two patents.



**Andrei M. Shkel** received the Diploma degree (with excellence) in mechanics and mathematics from Moscow State University, Moscow, Russia, in 1991, and the PhD degree in mechanical engineering from the University of Wisconsin, Madison, in 1997.

He was a postdoctoral researcher with the Berkeley Sensor and Actuator Center from 1997 to 1999. He then held research and consulting positions with several high-tech and venture companies. Since 2000, he has been a member of the faculty of the University of California, Irvine (UCI), where he is currently a Full Professor in the Department of Mechanical and Aerospace Engineering, Department of Electrical Engineering and Computer Sciences, and Department of Biomedical Engineering. He is also the Director of the UCI Microsystems Laboratory. He is the holder of twelve U.S. and international patents (with 15 pending) on micromachined angle-measuring gyroscopes, wide-bandwidth rate gyroscopes, design and fabrication of light manipulators and tunable optical filters, and hybrid micromachining processes. His professional interests, which are reflected in more than 100 publications, include solid-state sensors and actuators, microelectromechanical-system-based neuroprosthetics, sensor-based intelligence, and control theory.

Dr. Shkel is an editor of the *JOURNAL OF MICROELECTROMECHANICAL SYSTEMS*. He was a guest editor for two special issues of the *IEEE SENSORS JOURNAL*, the General Chair of the 2005 IEEE SENSORS Conference and the Vice General Chair and Publications Chair of the 2002–2006 IEEE Sensors Conferences. He served as the vice president of the IEEE Sensors Council from 2008 to 2009. Dr. Shkel is the recipient of the 2006 Research Award of the UCI School of Engineering, the 2005 National Science Foundation CAREER Award, the 2002 George E. Brown, Jr., Award, and a 2001 Fellowship from the Japanese Advanced Science Institute.